

# Antibodies From Children With PANDAS Bind Specifically to Striatal Cholinergic Interneurons and Alter Their Activity

Jian Xu, Ph.D., Rong-Jian Liu, Ph.D., Shaylyn Fahey, B.S., Luciana Frick, Ph.D., James Leckman, M.D., Ph.D., Flora Vaccarino, M.D., Ronald S. Duman, Ph.D., Kyle Williams, M.D., Ph.D., Susan Swedo, M.D., Christopher Pittenger, M.D., Ph.D.

**Objective:** Pediatric obsessive-compulsive disorder (OCD) sometimes appears rapidly, even overnight, often after an infection. Pediatric autoimmune neuropsychiatric disorders associated with streptococcal infections, or PANDAS, describes such a situation after infection with *Streptococcus pyogenes*. PANDAS may result from induced autoimmunity against brain antigens, although this remains unproven. Pilot work suggests that IgG antibodies from children with PANDAS bind to cholinergic interneurons (CINs) in the striatum. CIN deficiency has been independently associated with tics in humans and with repetitive behavioral pathology in mice, making it a plausible locus of pathology. The authors sought to replicate and extend earlier work and to investigate the cellular effects of PANDAS antibodies on cholinergic interneurons.

**Methods:** Binding of IgG to specific neurons in human and mouse brain slices was evaluated ex vivo after incubation with serum from 27 children with rigorously characterized PANDAS, both at baseline and after intravenous immunoglobulin (IVIG) treatment, and 23 matched control subjects. Binding was

correlated with symptom measures. Neural activity after serum incubation was assessed in mouse slices using molecular markers and electrophysiological recording.

**Results:** IgG from children with PANDAS bound to CINs, but not to several other neuron types, more than IgG from control subjects, in three independent cohorts of patients. Post-IVIG serum had reduced IgG binding to CINs, and this reduction correlated with symptom improvement. Baseline PANDAS sera decreased activity of striatal CINs, but not of parvalbumin-expressing GABAergic interneurons, and altered their electrophysiological responses, in acute mouse brain slices. Post-IVIG PANDAS sera and IgG-depleted baseline sera did not alter the activity of striatal CINs.

**Conclusions:** These findings provide strong evidence for striatal CINs as a critical cellular target that may contribute to pathophysiology in children with rapid-onset OCD symptoms, and perhaps in other conditions.

*Am J Psychiatry* 2021; 178:48–64; doi: 10.1176/appi.ajp.2020.19070698

Obsessive-compulsive disorder (OCD) occurs in 1% to 3% of children and adolescents in the United States, and a comparable fraction worldwide (1, 2). In a subset of pediatric OCD cases, onset of neuropsychiatric symptoms is strikingly abrupt; this has been termed pediatric acute-onset neuropsychiatric syndrome, or PANS (3, 4). In some children, symptom onset is temporally associated with an infectious illness, often with group A beta-hemolytic *Streptococcus* (GAS) (5). This natural history, and the presence of a constellation of characteristic associated symptoms (e.g., separation anxiety, severely restricted food intake, enuresis, choreiform movements, handwriting deterioration), suggests that this presentation may represent a discrete clinical entity, which has been termed “pediatric autoimmune neuropsychiatric disorders associated

with streptococcal infections,” or PANDAS. The incidence and prevalence of PANDAS are unknown. PANDAS and PANS have been the focus of considerable research, and some controversy, over three decades (5–7).

It has been suggested that PANDAS results from the postinfectious production of antibodies that target the basal ganglia, perhaps through the phenomenon of molecular mimicry (8, 9). This hypothesis draws an analogy to Sydenham chorea, a well-characterized poststreptococcal autoimmune neurological disorder in which comorbid OCD symptoms are often seen (5, 10–12). This pathophysiological hypothesis implies the presence of pathogenic anti-brain antibodies in children with PANDAS (13, 14). Indeed, autoantibodies against neuronal targets have been described in several studies, including

See related features: **Editorial** by Dr. Hyman (p. 5), **CME course** (online), and **Video** by Dr. Pine (online)

against lysoganglioside (15), tubulin (16), and dopamine D<sub>1</sub> and D<sub>2</sub> receptors (D1R and D2R) (17, 18). However, none of these binding patterns has been consistently replicated across studies. PANDAS sera have been shown to alter activation of calcium calmodulin protein kinase II in a human neuroblastoma cell line and to reduce cyclic adenosine monophosphate in a mouse fibroblast cell line expressing human D2R (15, 18).

Immune modulatory treatments such as plasmapheresis and intravenous immunoglobulin (IVIG) have shown promise in some trials, although others have been inconclusive (19–22). Antibiotic prophylaxis has also been found to be effective in reducing the rate of recurrent episodes in some studies (23), although again, others have not found clear benefit (24, 25). In animal studies, immunization with GAS can produce abnormal behavior, and passive transfer of sera from these GAS-exposed rodents to naive animals can recapitulate some of these abnormalities (26, 27). Thus, convergent evidence from multiple studies supports the concept of immunologic pathogenesis in PANDAS, but nonreplication has been common, and the literature has yet to converge on a clear understanding of the pathophysiology of the condition, or even whether it is appropriately conceived as a discrete entity.

The pathophysiology of OCD and tic disorders more broadly is incompletely understood (28, 29). Substantial evidence implicates dysregulation of cortico–basal ganglia circuits in both conditions (30–35), as well as in PANDAS. The striatum, which in primates consists of the caudate and putamen, is the primary input nucleus of the basal ganglia and integrates synaptic inputs from limbic and cortical regions (36). The vast majority of neurons in the striatum (~95% in rodents) consists of GABAergic medium spiny neurons. Only a small fraction (~5%) are interneurons (37), of which GABAergic interneurons are the most abundant. They can be classified on the basis of their expression of markers such as parvalbumin (PV), somatostatin, neuropeptide Y, and neuronal nitric oxide synthase (nNOS). A distinct, small population of large, tonically active cholinergic interneurons (CINs) is characterized by expression of choline acetyltransferase (ChAT). Although few in number, these interneurons are key regulators of striatal function (38–41). Both CINs and PV-expressing GABAergic interneurons are reduced in number in the caudate and putamen of individuals with Tourette's syndrome (42–44). Transcriptomic analysis of postmortem striatum from individuals with Tourette's syndrome similarly reveals reduced expression of interneuron-associated genes (43). Experimental depletion of these cells in developmentally normal mice produces repetitive behavioral pathology (45, 46), suggesting that this neuronal deficit is causally related to symptomatology.

In a small initial study (N=5), we found that IgG antibodies from children with rigorously characterized PANDAS showed significantly higher *in vivo* binding to CINs in mouse than IgG from age- and gender-matched healthy control subjects. This elevated IgG binding to CINs resolved in parallel with symptom improvement in serum collected after IVIG treatment (47). This suggests that binding of IgG to striatal CINs may contribute to pathophysiology in PANDAS.

Here, we confirmed elevated IgG binding to CINs, but not to other striatal neurons, both in the original five PANDAS patients in our pilot study and in two additional independent cohorts of patients, and in both mouse and human striatal tissue. Reduced IgG binding to CINs correlated with symptom improvement after IVIG treatment (21, 47). Furthermore, PANDAS serum reduced molecular markers of spontaneous activity of CINs, but not of PV-expressing interneurons, in an *ex vivo* assay, and reduced the electrophysiological response of CINs to the glutamate agonist  $\alpha$ -amino-3-hydroxy-5-methyl-4-isoxazolepropionic acid (AMPA), compared with matched control serum. Post-IVIG sera and IgG-depleted baseline sera did not alter activity of CINs, suggesting that serum IgG is necessary for the cellular effects. These data reveal a novel mechanism whereby specific antibodies in children with PANDAS can bind to and inhibit CINs, which may contribute to symptoms.

## METHODS

### PANDAS Serum

These investigations of human serum samples were approved by the Human Investigations Committees of Yale University and the National Institute of Mental Health (NIMH). Parents gave written informed consent for participation in the study, and children gave assent. In the first two cohorts of patients analyzed, sera from 11 children with a well-substantiated diagnosis of PANDAS were selected from a clinical trial performed at NIMH and Yale University (ClinicalTrials.gov identifier, NCT01281969), as described previously (21). Participants met rigorous clinical and laboratory criteria for a diagnosis of PANDAS (5) and were additionally selected for having a robust clinical response to treatment with intravenous immunoglobulin (IVIG) (21); we reasoned that IVIG responders are most likely to have antibody-mediated pathology. The Children's Yale-Brown Obsessive Compulsive Scale (CY-BOCS) (48) was administered at baseline (before IVIG treatment) and at 6, 12, and 18 weeks; serum from the baseline and 12-week visits (visits 1 and 3 in the clinical trial; see Figure S1 in the online supplement) were used in the present study. The mean CY-BOCS score was 28.64 (SD=3.41) at baseline and 5.64 (SD=5.26) at 3 months, after one or two rounds of IVIG treatment. Samples from a third cohort of 16 PANDAS patients and 12 matched control subjects were obtained from the same NIMH PANDAS clinic; these samples were drawn from several different studies and were not preselected for IVIG response. Samples from age- and gender-matched healthy subjects with no clinically significant OCD or tic symptoms were collected by the same investigators at NIMH and were stored and tested in parallel. The first patient cohort, consisting of five PANDAS patients and five matched control subjects, has been described previously (47). All samples were aliquoted into small volumes on arrival at Yale University and stored at  $-80^{\circ}\text{C}$  until use. Demographic data for all participants are summarized in Tables S1 and S2 in the online supplement. All sera were coded before being

sent from NIMH to Yale University for analysis, and all analyses were performed blind to diagnosis and treatment condition.

### Normal Human Brain Tissue

The collection and preparation of formalin-fixed normal human brain tissue have been described previously (43). Coronal sections of caudate and putamen (50  $\mu$ m, two sections per serum) were used for serum antibody binding and immunostaining, as further detailed below.

### Animals

All experimental procedures were approved by the Yale University Institutional Animal Care and Use Committee, in accordance with the National Institutes of Health (NIH) Guide for the Care and Use of Laboratory Animals. Male and female C57BL/6J mice were purchased from the Jackson Laboratory (Bar Harbor, Me.). Double-transgenic D1-DARPP-32-FLAG/ D2-DARPP-32-Myc were backcrossed to C57BL/6J for at least nine generations and have been described previously; the transgenically expressed FLAG and Myc epitope tags allow dissociable immunostaining of D1R- and D2R-expressing medium spiny neuron populations (49, 50). All mice were maintained on a 12-hour light/dark cycle and used at 3–6 months of age.

### Reagents and Antibodies

N-methyl-D-glucamine (NMDG), glucose, thiourea, sodium pyruvate, sodium ascorbate, tetrodotoxin (TTX), Sudan Black B, and Triton X-100 were obtained from Sigma (St. Louis, Mo.). Dopamine and other chemicals used for electrophysiology (see Figure S12 in the online supplement) were also obtained from Sigma, with the exception of 5-HT and AMPA, which were obtained from Tocris (Ellisville, Mo.). Paraformaldehyde, KCl, and other chemicals used for acute brain slice analysis were obtained from J.T. Baker Chemical Co. (Phillipsburg, N.J.). Ketamine was obtained from Zoetis (Madison, N.J.). Xylazine was obtained from Akorn, Inc. (Decatur, Ill.). Antibodies used in immunohistochemical staining are listed in Table S3 in the online supplement.

### Determination of Serum IgG Titer and IgG Depletion

Total IgG titers in control and PANDAS sera were determined using the IgG (Total) Human ELISA Kit (Thermo Scientific, Rockland, Ill.), following the manufacturer's instructions. Prediluted sera were added to microplates pre-coated with an anti-human IgG capture antibody and incubated for 2 hours at room temperature. After washes, a horseradish peroxidase (HRP)-conjugated anti-human IgG detection antibody was added for 1 hour at room temperature. After extensive washes, 3,3',5,5'-tetramethylbenzidine solution was added to each well for 15 minutes. The reaction was stopped with 1 M phosphoric acid and optical density reading was obtained using an MQX200  $\mu$ Quant plate reader (BioTek, Winooski, Vt.) at 450 nm. Human IgG standard provided in the kit was used as a reference to determine IgG concentration

in each serum. All sera were diluted in 1 $\times$  phosphate-buffered saline (PBS) + 0.1% bovine serum albumin to 500 mg/dL IgG.

For IgG depletion, baseline (pre-IVIG treatment) PANDAS sera from 11 patients (see Table S1 in the online supplement) were incubated with Protein A/G agarose beads (Thermo Scientific) for 2 hours at 4°C. Supernatants were collected by brief centrifugation (1000 $\times$ g for 1 minute). Supernatants were mixed with fresh Protein A/G agarose beads for a second round of depletion. To confirm IgG depletion, small aliquots from both batches of supernatants were tested on dot blot using a rabbit anti-human IgG antibody (Abcam, Cambridge, Mass.) and HRP-conjugated goat anti-rabbit secondary antibody (Thermo Scientific). Membranes were developed using the Chemiluminescent Substrate kit (Thermo Scientific) and visualized on a ChemiDoc XRS+ system (Bio-Rad, Hercules, Calif.).

### Immunohistochemistry

Mice were anesthetized by intraperitoneal injection of ketamine (100 mg/kg) with xylazine (10 mg/kg) and transcardially perfused with cold 4% paraformaldehyde in 1 $\times$ PBS (pH 7.4). Brains were fixed overnight in 4% paraformaldehyde at 4°C, followed by equilibration in 30% sucrose for 48 hours at 4°C. Striatal slices were cut at 20  $\mu$ m using a Leica CM3050S cryostat (Leica, Buffalo Grove, Ill.). Slices were stored in a cryoprotectant solution (30% glycerin, 30% ethylene glycol in 1 $\times$ PBS, pH 7.4) at –20°C until use. All staining was done using wild-type (WT) C57BL6 mice, except for examination of D1R- and D2R-expressing medium spiny neurons, for which we used D1-FLAG/D2-Myc double-transgenic mice (49, 50).

Brain sections were washed three times, 10 minutes each time (3 $\times$ 10 minutes), in 1 $\times$ PBS (pH 7.4) to remove cryoprotectant, followed by incubation in freshly prepared 0.1% Sudan Black (in 70% ethanol) for 10 minutes at room temperature to reduce autofluorescence. Slices were washed 3 $\times$ 10 minutes in 70% ethanol and 3 $\times$ 10 minutes in 1 $\times$ PBS. Slices were blocked in 1 $\times$ PBS+0.3% Triton X-100 supplemented with 5% donkey serum (Jackson ImmunoResearch, West Grove, Pa.) for 1 hour at room temperature and then incubated overnight at 4°C with PANDAS or healthy control serum at 1.25 mg/dL (diluted in blocking buffer; this dilution was found in extensive pilot experiments to provide an optimal signal-to-noise ratio for cell body staining). For staining with mouse primary antibodies (anti-PV, anti-nNOS, and anti-FLAG), slices were additionally blocked in Mouse-on-Mouse reagent (Vector Laboratories, Burlingame, Calif.), following the manufacturer's instructions. Slices were then washed 3 $\times$ 10 minutes in 1 $\times$ PBS+0.3% Triton X-100 and incubated with primary antibodies (see Table S3 in the online supplement) in blocking buffer overnight at 4°C. Sections were double-immunostained with anti-human IgG to identify serum IgG binding (green) and selected neuronal markers (ChAT, PV, nNOS, and antibodies to the epitope tags FLAG and Myc to detect medium spiny neurons in

D1-DARPP-32-FLAG/D2-DARPP-32-Myc; red). The next day, slices were washed 3×10 minutes in 1×PBS+0.3% Triton X-100 and then incubated with fluorophore-conjugated secondary antibodies (see Table S3) for 1 hour at room temperature. After 3×10 minute washes in 1×PBS, slices were mounted in Vectashield HardSet Mounting Medium (Vector Laboratories), coverslipped, and stored at 4°C.

For illustrative purposes, IgG binding was visualized by sequential scanning of slices on an Olympus Fluoview FV-1000 confocal microscope with a 40×/1.30 NA objective (Olympus, Japan; Figures 1A, 3A, 3F, and 4A, and corresponding high-magnification panels in the supplementary figures).

For quantification, we used lower-magnification images collected using single-photon fluorescence imaging; these images are of lower resolution than confocal images and do not resolve the z-dimension as well, but they allow us to quantify an order of magnitude more cells (see Figures S2 and S16–S19 in the online supplement). Single-photon fluorescence images were collected using an Axioskop 2 fluorescent microscope with a 20×/0.8 NA objective (Zeiss, Oberkochen, Germany) or an Axio Scope A1 fluorescent microscope with a 10×/0.45 NA objective (Zeiss). We took 36–48 images from four to six mice per serum in the dorsal striatum and 12–16 images from four to six mice for each serum in the medial septum. Microscope settings were kept constant (2500–3500 ms exposure for IgG images and 1000–1500 ms for neuronal markers: ChAT, PV, nNOS, FLAG, and Myc) across all images between which comparisons were made. In some cases (Figure 1; see also Figure S6 in the online supplement), because of limited microscope availability, images were captured using different microscopes for different cohorts. To compensate for differences in background binding across experiments, data were normalized to the mean value of the control samples processed in the same batch. Microscope fields were chosen without overlap within dorsal striatum, using the lateral ventricle as an anatomical landmark, to ensure that comparable fields were examined for all sera; the distribution of images and the total number of cells of each type quantified are shown in Figure S2 in the online supplement. Cell counts did not differ between PANDAS and control groups for any neuron type.

Human brain sections were triple-immunostained with anti-human IgG and markers for ChAT and PV, following the same protocol. Three-color images were collected using an Olympus Fluoview FV-1000 confocal microscope with a 40×/1.30 NA objective. Triple-staining and confocal imaging limit the number of cells quantified but were used for this experiment to permit triple-labeling and thereby conserve human tissue samples.

#### Acute Brain Slice Preparation, Ex Vivo Serum Treatment, and Quantification of Phospho-rpS6

For the functional assay shown in Figures 3 and 5, acute brain slices were prepared from male and female wild-type mice and treated ex vivo with PANDAS serum (pre-IVIG, post-IVIG, and IgG-depleted pre-IVIG) or control serum. Mice

were sacrificed by cervical dislocation; brains were quickly removed and placed in ice-cold oxygenated NMDG-based artificial cerebrospinal fluid (aCSF), as previously described (51). We cut 100 μm coronal slices through the striatum (see Figure S2 in the online supplement) using a Leica VT1000S vibratome (Leica Microsystems, Bannockburn, Ill.) in the NMDG solution containing (in mM) 92 NMDG, 2.5 KCl, 1.25 NaH<sub>2</sub>PO<sub>4</sub>, 30 NaHCO<sub>3</sub>, 20 HEPES, 10 MgSO<sub>4</sub>, 0.5 CaCl<sub>2</sub>, 25 glucose, 2 thiourea, 3 sodium pyruvate, and 5 sodium ascorbate, pH 7.35, saturated with 95% O<sub>2</sub>/5% CO<sub>2</sub>.

Slices were recovered in NMDG-aCSF for 10 minutes at 32°C before being transferred to regular aCSF containing (in mM) 119 NaCl, 2.5 KCl, 1.25 NaH<sub>2</sub>PO<sub>4</sub>, 24 NaHCO<sub>3</sub>, 2 CaCl<sub>2</sub>, 2 MgSO<sub>4</sub>, and 12.5 glucose for 1 hour at 30°C under constant oxygenation with 95% O<sub>2</sub>/5% CO<sub>2</sub>. After recovery, slices were treated with control drugs (TTX 1 μM; KCl 20 mM; 0.1% dimethyl sulfoxide (DMSO) in aCSF), control serum (1.25 or 6.25 mg/dL), or PANDAS serum (baseline, post-IVIG, or IgG-depleted baseline; 1.25 or 6.25 mg/dL) for 1 hour at 30°C. A subset of slices were treated with aCSF with 0.1% DMSO in each experiment; data from other conditions were normalized to this vehicle condition for analysis. After treatment, slices were fixed in cold 4% paraformaldehyde in 1×PBS (pH 7.4) containing 5 mM NaF for 1 hour at 4°C.

Sections shown in Figure 3 were double-immunostained for phospho-rpS6 (green) and ChAT (red) or PV (red), as described above. For ChAT/P-rpS6 staining, 23–56 images from four to seven mice were taken in the dorsal striatum for each serum and 100–350 CINs were quantified for each serum. For PV/P-rpS6 staining, 40–52 images from five mice were taken in the dorsal striatum and 60–100 PV<sup>+</sup> interneurons were quantified for each serum. Total cells counted did not differ between PANDAS and control groups. Sections shown in Figure 5 were triple-immunostained with anti-human IgG, anti-ChAT, and anti-PV, as described above. Images were collected using an Olympus Fluoview FV-1000 confocal microscope with a 40×/1.30 NA objective. Triple-immunostaining and confocal imaging limit the number of cells quantified but were used for this experiment to conserve serum.

#### Image Processing and Quantification

Automated quantitation of mean fluorescence intensity within each cell was achieved using Fiji ImageJ from NIH (<https://imagej.net/Fiji/Downloads>) with batch processing, as illustrated in Figure S3 in the online supplement. Neuronal marker immunostaining (ChAT, PV, N-NOS, FLAG, or c-Myc) was thresholded and used to generate regions of interest corresponding to cell bodies of the selected cell type. The number and spatial extent of these cellular regions of interest were quantified to ensure between-group comparability. The total regions of interest per section obtained for each serum was interpreted as cell number for the selected cell type. This spatial filter was then overlaid on the corresponding anti-human IgG or phospho-rpS6 image, and immunostaining within each cellular region of interest was quantified.

Background IgG or phospho-rpS6 signal was subtracted to generate an adjusted value for each cell. This procedure is illustrated in Figure S3. Although this procedure is wholly automated, serum identity was coded until all the values were retrieved, as an additional safeguard for the rigor of the analysis.

### Brain Slice Electrophysiology

Brain slices were prepared as previously described (52). Briefly, mice were anesthetized using chloral hydrate (400 mg/kg i.p.) and brains were removed and placed in ice-cold aCSF in which sucrose (252 mM) was substituted for NaCl (sucrose-aCSF). A block of tissue containing corticostriatal and coronal slices (400  $\mu$ m) was cut in sucrose-aCSF with an oscillating-blade tissue slicer. After 60 minutes' incubation with normal or PANDAS sera (6.25 mg/dL) in standard aCSF containing (in mM) 128 NaCl, 3 KCl, 2 CaCl<sub>2</sub>, 2 MgSO<sub>4</sub>, 24 NaHCO<sub>3</sub>, 1.25 NaH<sub>2</sub>PO<sub>4</sub>, and 10 D-glucose (pH 7.35–7.38) equilibrated with 95% O<sub>2</sub>/5% CO<sub>2</sub> at room temperature, slices were transferred into a submerged recording chamber; bath temperature was then raised to 32°C. Patch pipettes (3–5 M $\Omega$ ) were pulled from glass tubing with a Flaming-Brown horizontal puller. The pipette solution contained the following (in mM): 115 K-gluconate, 5 KCl, 2 MgCl<sub>2</sub>, 2 Mg-ATP, 2 Na<sub>2</sub>-ATP, 10 Na<sub>2</sub>-phosphocreatine, 0.4 Na<sub>2</sub>-GTP, and 10 HEPES, pH 7.33. Neurobiotin (0.3%) was added to the pipette solution to mark cells for later imaging. All drugs, in aCSF, were applied for 1.5 minutes at a time in the fast-flowing bath, followed by a washout period of 8–10 minutes.

Cholinergic interneurons in striatum were visualized by videomicroscopy (40 $\times$ IR lens) with infrared differential interference contrast and selected on the basis of their size and characteristic morphology. Whole-cell recordings were performed with an Axoclamp-2B amplifier. Postsynaptic currents were studied in the continuous single-electrode voltage-clamp mode (3000 Hz low-pass filter) clamped at –70 mV. Spontaneous or neurotransmitter (5-HT, AMPA, and dopamine) evoked spike and intrinsic membrane properties were determined using current clamp. Analysis of spike frequency and inward current was conducted with Clampfit, version 10 (Molecular Devices, Sunnyvale, Calif.).

### Data Analysis

All data are expressed as means and standard deviations. Statistical analyses were performed using SPSS Statistics, version 24 (IBM, Armonk, N.Y.) or Prism, version 7.0 (GraphPad Software, La Jolla, Calif.). Significance ( $p < 0.05$ ) was determined by two-tailed t test (unpaired or paired), one-sample t test, or one-way or two-way analysis of variance with post hoc Tukey's test. Specific tests used in each analysis are listed in the figure legends. The unit of analysis (patient/serum, mouse, slice, or cell) is indicated for individual analyses. Pearson correlation was used to examine linear relationships between measures. For electrophysiology, the mean discharge frequency at 30 seconds before administration and 30 seconds after administration was compared and statistically analyzed.

## RESULTS

### Specifically Elevated Binding of PANDAS IgG to Mouse Striatal CINs

In our recent study, we examined the binding of IgG from five children with PANDAS to striatal interneurons after infusion of human sera into the brains of mice *in vivo*, and found elevated binding specifically to CINs (21, 47). Here, we developed an *ex vivo* approach to replicate and extend this pilot work, equalizing IgG titers across samples and using blinded, unbiased imaging with automated scoring (see Methods).

We first tested the five PANDAS and five control samples characterized in our pilot study using this *ex vivo* assay; this constitutes a technical replication of our previous work (47). Mouse CINs were identified using an anti-choline acetyltransferase (ChAT) antibody; deposition of serum IgG onto these cells was visualized using a specific anti-human IgG antibody. IgG from both PANDAS and control sera bound to striatal mouse CINs (see Figures S4A and S16A in the online supplement). We quantified IgG immunofluorescence within all visualized ChAT-positive cells for each serum (400–800 cells/serum across multiple microscope fields). IgG immunofluorescence followed a normal distribution for each serum, but the distribution of binding by PANDAS antibodies was shifted to the right, indicating more deposition of PANDAS antibodies onto CINs (see Figure S4B in the online supplement). Comparison of mean CIN IgG immunofluorescence for each serum confirmed significantly higher antibody binding in the PANDAS group (see Figure S4C in the online supplement). *Ex vivo* binding scored in this way correlated positively, albeit imperfectly, with binding scored manually after *in vivo* infusion of the same sera in our previous work ( $r^2 = 0.373$ ,  $p = 0.061$ ; not shown) (47). There was no between-group difference in ChAT immunofluorescence (data not shown), indicating that PANDAS and control sera did not differentially affect ChAT antibody binding.

Next, we investigated binding of serum IgG to other types of mouse interneuron. In PV-positive interneurons, PANDAS and control serum displayed similar IgG deposition (see Figures S4D and S16B in the online supplement), with no between-group difference (see Figure S4E,F in the online supplement). In nNOS-positive interneurons, PANDAS and control sera bound similarly (see Figures S4G–I and S16C in the online supplement). Together these results replicate our previous finding (47) that PANDAS serum IgG shows selectively elevated binding to CINs in this small number of rigorously characterized patient samples.

### Independent Replication of Binding of PANDAS IgG to CINs in Two Additional Cohorts of Patients

To test the generality of this finding, we performed the same analyses in two independent cohorts of patients and control subjects. The second cohort consisted of six children with PANDAS and six age- and gender-matched control subjects (subjects 6–11 in Table S1 in the online supplement). PANDAS cases were again drawn from a recent trial of IVIG treatment

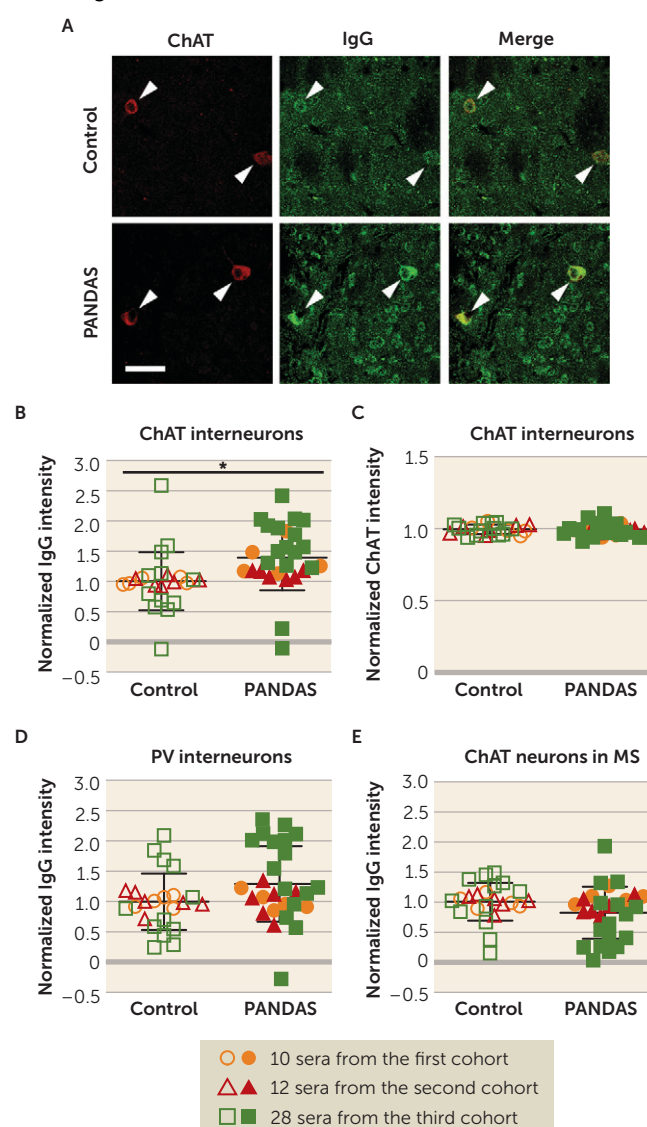
(21) and were selected to be clinical responders after either blinded or open-label IVIG. The third cohort consisted of 16 children with PANDAS and 12 age- and gender-matched control subjects collected by the same group (S.S. and the NIMH PANDAS clinic; see Table S2). Participants in the third cohort were not selected to be treatment responders; indeed, many of them were not treated with IVIG. Consistent with the findings in the first five cases, IgG from both PANDAS and control sera bound to mouse striatal CINs (Figure 1A). Combined data from all three cohorts (27 PANDAS patients and 23 control subjects) showed a robust and significant group difference, with elevated binding of IgG from PANDAS samples relative to control subjects (Figure 1B). The level of ChAT immunofluorescence was unchanged between groups (Figure 1C), indicating no differential effect on anti-ChAT antibody binding. The number of ChAT-positive cells scored in the mouse striatum did not differ between PANDAS IgG and control IgG-treated groups (see Figure S5A in the online supplement).

Binding of serum IgG to PV-positive interneurons did not differ significantly between PANDAS patients and control subjects in pooled data from all three cohorts (Figure 1D). There was no difference between groups in the number of PV-positive cells or PV staining per cell (see Figure S5B,C in the online supplement).

To determine whether this elevated binding is seen in all cholinergic neurons, we next examined serum IgG binding to cholinergic neurons in the mouse medial septum. IgG immunofluorescence was seen in these cholinergic neurons (see Figure S16D in the online supplement), but there was no difference between groups (Figure 1E). There was no difference between groups in the number of ChAT-positive cells or the intensity of ChAT immunofluorescence per cell (see Figure S5D,E in the online supplement).

We also examined antibody binding of sera from the first and second cohorts (11 PANDAS patients and 11 control subjects) to other cells in the striatum. IgG from PANDAS and control sera bound similarly to nNOS-expressing interneurons (see Figure S6A in the online supplement). There was no difference between groups in the number of nNOS-positive cells or nNOS staining per cell (see Figure S6B,C). A few previous studies have suggested that PANDAS serum antibodies may bind to D1R and D2R (8, 18). We tested whether IgG in PANDAS serum would show altered binding to striatal medium spiny neurons (MSNs) expressing D1R or D2R. To distinguish D1R- and D2R-expressing MSNs, we used double-transgenic mice expressing transgenic DARPP-32 with a FLAG epitope tag in DR1 MSNs and with a Myc epitope tag in DR2 MSNs (49), as in our recent work (50, 53). Double-labeling for epitope tags (FLAG or Myc) and human IgG (see Figure S17A,B in the online supplement) allows cell type-specific quantification of IgG binding, using the *ex vivo* approach described above for interneurons. Binding of IgG from PANDAS and control sera to D1R MSNs (see Figure S6D in the online supplement) and D2R MSNs (see Figure S6G) was equivalent. There was no difference between groups in FLAG or Myc

**FIGURE 1. Elevated binding of PANDAS IgG to mouse striatal cholinergic interneurons<sup>a</sup>**



<sup>a</sup> Panel A presents illustrative confocal images of immunohistochemical staining of human IgG (green) and choline acetyltransferase (ChAT) (red). “Merge” images combine both channels to illustrate overlap. Arrowheads indicate human IgG binding to ChAT-positive neurons (cholinergic interneurons, CINs). Scale bar: 40  $\mu$ m. In panel B, the average intensity of IgG binding to CINs was higher after incubation with PANDAS sera than after incubation with control sera (two-tailed independent-sample t test,  $t=2.670$ ,  $df=48$ ,  $p=0.010$ ). This was true in separate analyses of each of the three cohorts of patients (first cohort:  $t=2.810$ ,  $df=8$ ,  $p=0.023$ ; second cohort:  $t=2.785$ ,  $df=10$ ,  $p=0.019$ ; third cohort:  $t=1.958$ ,  $df=26$ ,  $p=0.061$ ). In panel C, the mean intensity of ChAT immunofluorescence did not differ between the two groups ( $t=0.136$ ,  $df=48$ ,  $p=0.9$ ). In panels D and E, serum IgG binding to several other neuron types did not significantly differ between PANDAS and control groups (parvalbumin [PV]-expressing interneurons:  $t=1.853$ ,  $df=48$ ,  $p=0.070$ ; ChAT-positive neurons in the medial septum [MS]:  $t=1.688$ ,  $df=48$ ,  $p=0.098$ ).  $N=27$  for the PANDAS group and  $N=23$  for the control group. The first cohort was independently characterized in our previous pilot study (47). \* $p<0.05$ .

staining per cell (see Figure S6E,H) or in the number of FLAG-positive or Myc-positive cells (see Figure S6F,I). These controls, including three cell types not examined in our previous work (47) (septal cholinergic neurons and D1R-expressing and

D2R MSNs), further confirm the specificity of elevated PANDAS antibody binding to CINs.

### **Elevated Binding of PANDAS IgG to CINs, But Not to PV-Expressing Interneurons, in Normal Human Brains**

To confirm these findings in human brain, we examined the binding of IgG from PANDAS and control sera to slices of human basal ganglia of normal subjects. Pilot studies were carried out to optimize staining conditions (see Figure S7 in the online supplement). Sera from the first two cohorts (11 PANDAS patients and 11 control subjects) were incubated with slices of human caudate and putamen and then co-immunostained for human IgG, ChAT, and PV. IgG binding to CINs was elevated after incubation with PANDAS serum compared with the control serum in the caudate (Figure 2A,B) and putamen (Figure 2C,D). There was no between-group difference in IgG binding to PV-positive interneurons in the caudate (Figure 2E,F) or putamen (Figure 2G,H). Serum incubation did not alter ChAT or PV immunofluorescence (not shown).

### **Reduction of CIN Activity by PANDAS Serum**

CINs regulate motor function (54, 55) and have been found to be reduced in number in postmortem brain from adults with Tourette's syndrome (42, 43). Selective depletion of CINs in mice produces repetitive behavioral pathology (45, 56). We used phosphorylation levels of ribosomal protein S6 (rpS6) as a readout for CIN activity (as previously described [57]) in mouse striatal slices acutely treated with control or PANDAS sera (see Figures S8, S9, and S18A in the online supplement) to test whether binding by PANDAS antibodies affects CIN function. All values were normalized to P-rpS6 in CINs treated in parallel with saline.

We tested the 11 PANDAS sera and 11 matched control sera for modulation of CIN activity in this assay. Control serum did not significantly alter P-rpS6 relative to vehicle. PANDAS serum treatment significantly lowered P-rpS6 levels relative to control serum (Figure 3A,B; see also Figure S18B in the online supplement). ChAT immunostaining was not significantly changed by serum treatment (Figure 3C), nor was the number of ChAT-positive cells (data not shown).

Across all 22 samples, serum IgG binding to CINs correlated negatively with CIN P-rpS6 activity after serum treatment (Figure 3D). The difference between PANDAS and control IgG binding to CINs in each age- and gender-matched serum pair correlated with the PANDAS-control difference in P-rpS6 after serum incubation (Figure 3E). These associations suggest that PANDAS IgG binding negatively regulates the activity of striatal CINs.

To test the specificity of this change, we investigated whether PANDAS serum affected the activity of PV-positive interneurons, again measured by immunostaining for P-rpS6 (58, 59), in striatal slices (see Figures S10 and S18C in the online supplement). PANDAS and control serum-treated striatal slices showed similar levels of P-rpS6 in PV-interneurons (Figure 3F,G; see also Figure S18D). Serum treatment did not alter

PV immunostaining relative to saline (Figure 3H). No correlation was found between serum IgG binding to PV-interneurons and P-rpS6 levels (Figure 3I) or between the difference between PANDAS and matched control IgG binding to PV-interneurons and the difference in PV P-rpS6 levels (Figure 3J).

### **Alteration of CIN Electrophysiological Responses by PANDAS Serum**

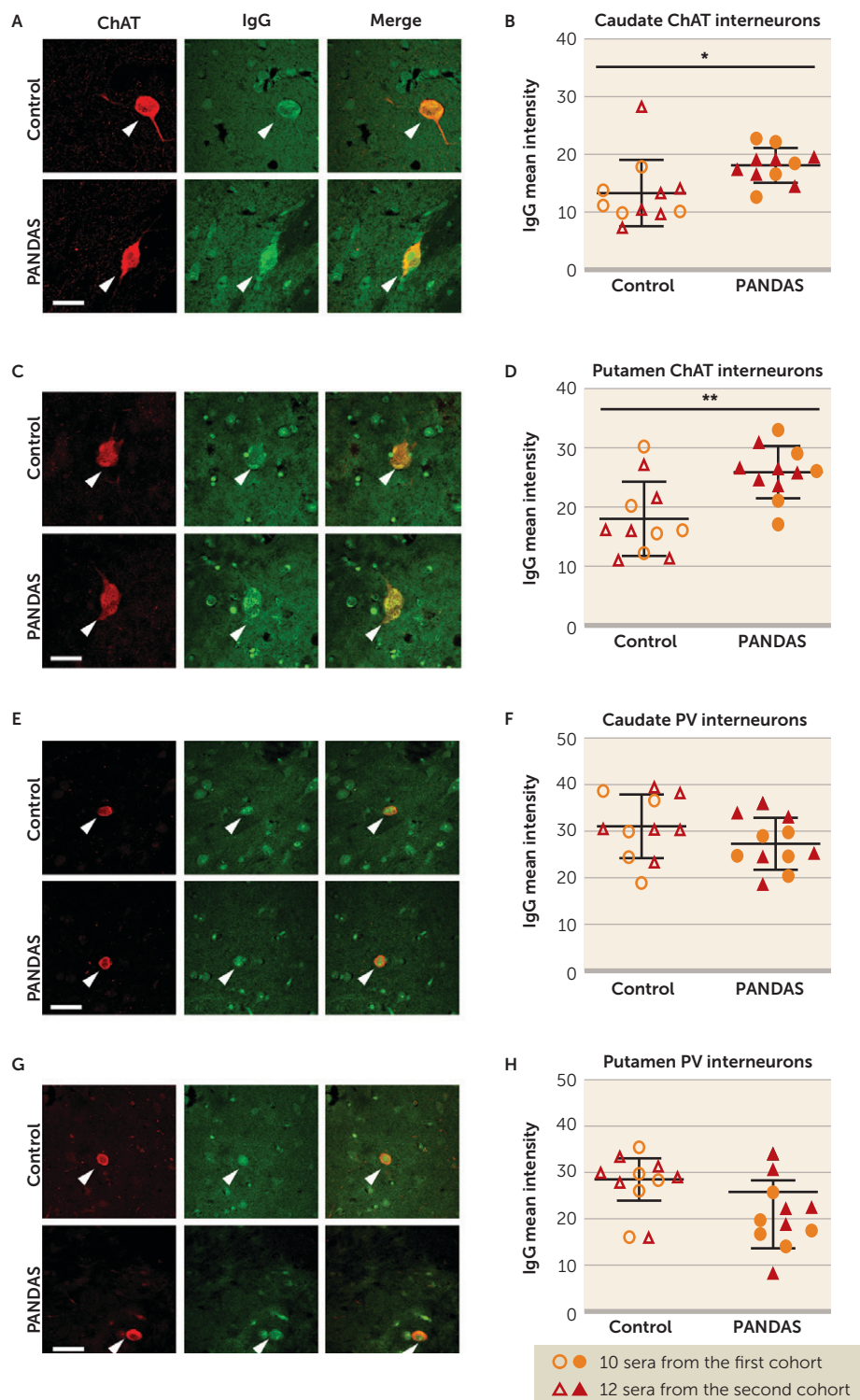
We used whole-cell patch recording to further examine the effect of PANDAS serum on CIN activity in acute brain slices. These experiments require much larger serum volumes than the immunostaining described above (Figure 3), and we were thus only able to conduct them with a single PANDAS-control serum pair for which we had adequate volumes of serum. CINs were identified on the basis of their electrophysiological and morphological characteristics, including large somata and hyperpolarizing current pulses evoking a prominent voltage sag, characteristic of an  $I_h$  current (see Figure S11A,B in the online supplement). Most recorded neurons displayed spontaneous spiking, with relatively broad action potentials (see Figure S11C,D). PANDAS and control sera did not differentially affect intrinsic membrane properties of cholinergic interneurons (see Table S4 in the online supplement).

CINs receive various synaptic inputs, including glutamate, dopamine, and serotonin (5-HT) (54). We therefore examined their response to bath application of agonists for these receptors. In slices pretreated with control serum, application of the ionotropic glutamate agonist AMPA produced a robust increase in action potential frequency in CINs, measured under current clamp. This increase did not occur in slices pretreated with PANDAS serum (see Figure S12A,B in the online supplement). Alterations were also seen in the response of CINs to dopamine and 5-HT after pretreatment with PANDAS serum (see Figure S12C-F). Under voltage clamp, inward current was seen after application of all three agonists; the current induced by 5-HT was significantly reduced after pretreatment with PANDAS serum, while responses to AMPA and dopamine were not significantly altered (see Figure S13 in the online supplement). These electrophysiological data must be interpreted with caution, as we were able to perform these assays with only a single serum pair; with that caveat, they support the molecular data (Figures 3 and 5) indicating that pretreatment with PANDAS serum can reduce the firing and/or responsiveness of CINs *ex vivo*.

### **IVIg Treatment Reduces Binding of PANDAS IgG to CINs**

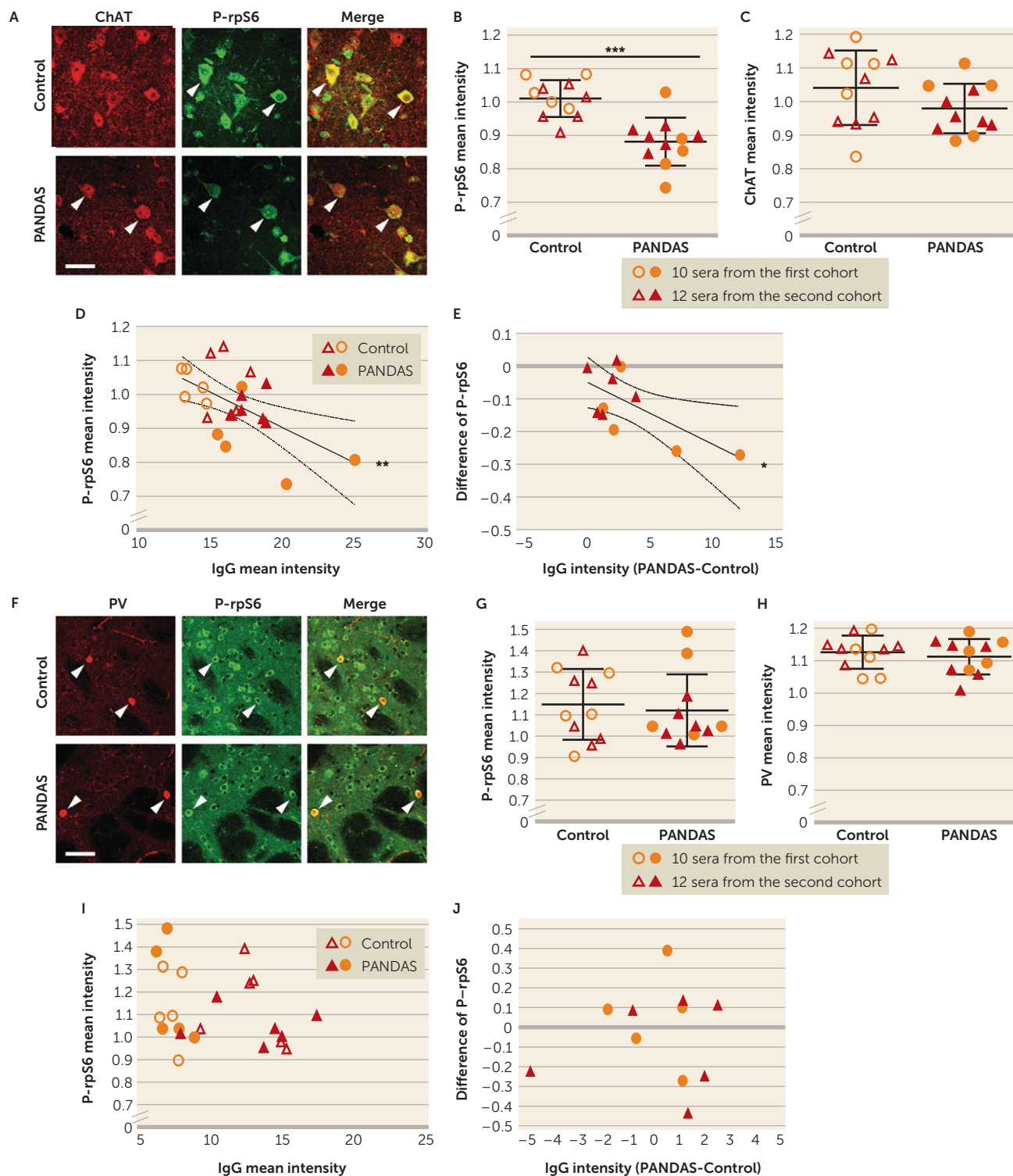
IVIg treatment has been reported to ameliorate symptoms in PANDAS, in some studies (19, 21, 60); the first two patient cohorts in the present study were selected on the basis of their clinical response 6–12 weeks after either blinded or open-label IVIg treatment (see Figure S1 in the online supplement). We examined the correlation of change in CIN binding with change in symptoms after IVIg. In the original cohort of five patients, posttreatment serum showed a small but

**FIGURE 2. Elevated binding of PANDAS IgG to cholinergic interneurons in human brain slices<sup>a</sup>**



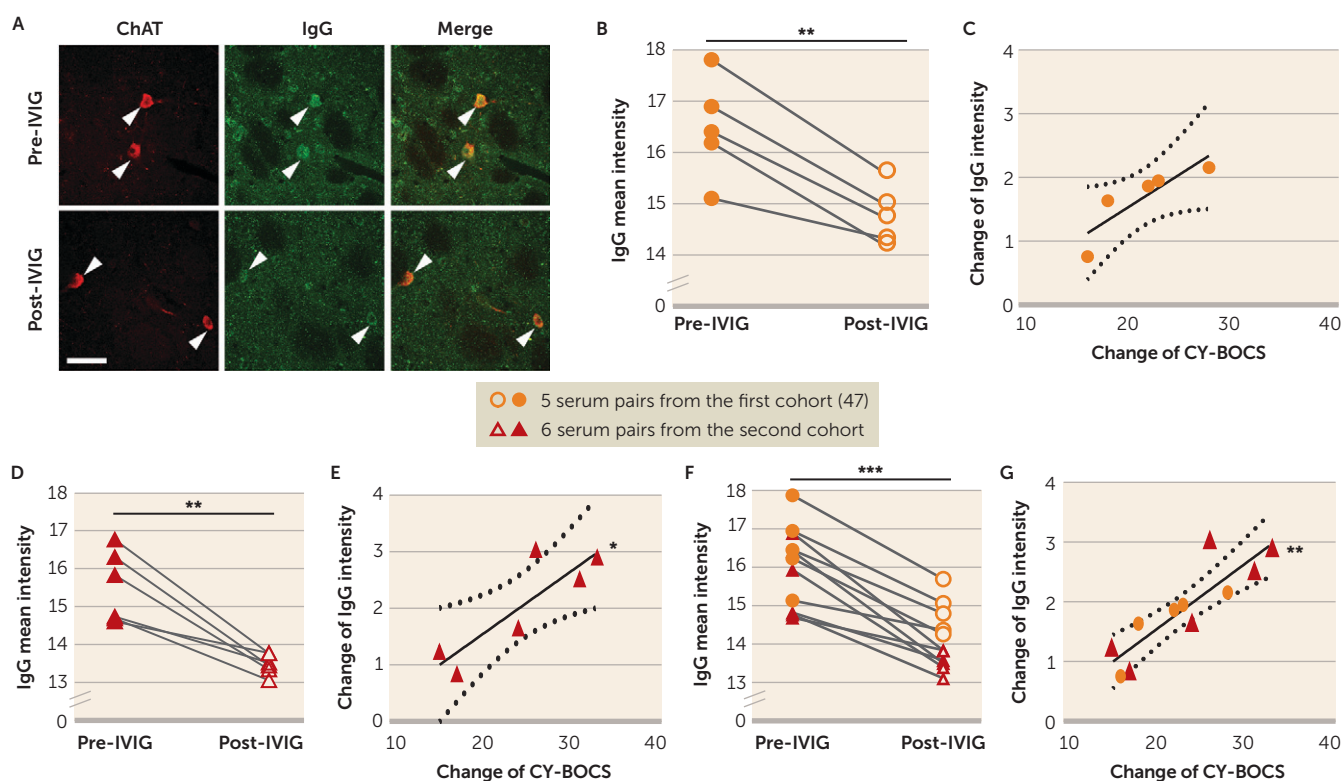
<sup>a</sup> Panels A and C present representative confocal images of immunohistochemical staining of human IgG (green) and choline acetyltransferase (ChAT) (red) in human caudate (panel A) and putamen (panel C). “Merge” images combine both channels to illustrate overlap. Arrowheads indicate human IgG binding to cholinergic interneurons (CINs). Scale bar: 40  $\mu$ m. In panels B and D, PANDAS antibodies show more binding to CINs in human caudate and putamen, relative to matched controls, as quantified by average fluorescence intensity (caudate,  $t=2.440$ ,  $df=20$ ,  $p=0.024$ ; putamen,  $t=3.401$ ,  $df=20$ ,  $p=0.003$ ). Panels E and G present representative confocal images of immunohistochemical staining of human IgG (green) and parvalbumin (PV) (red) in human caudate (panel E) and putamen (panel G). Arrowheads indicate human IgG binding to PV-positive interneurons. Scale bar: 40  $\mu$ m. In panels F and H, PANDAS antibodies do not show elevated binding to PV-positive interneurons (caudate,  $t=1.409$ ,  $df=20$ ,  $p=0.174$ ; putamen,  $t=1.042$ ,  $df=20$ ,  $p>0.3$ ). The first cohort was independently characterized in our previous pilot study (47). All comparisons are by independent-samples t test;  $N=11$  for each group. \* $p<0.05$ . \*\* $p<0.01$ .

**FIGURE 3. Association of PANDAS serum and reduced spontaneous activity in striatal cholinergic interneurons in acute mouse brain slices<sup>a</sup>**



<sup>a</sup> Panel A presents confocal images of co-staining of anti-phospho-rpS6 (green) and anti-ChAT (choline acetyltransferase) (red) in striatal slices after PANDAS or control serum incubation. “Merge” images combine both channels to illustrate overlap. Arrowheads indicate P-rpS6/ChAT co-labeled cholinergic interneurons (CINs). Scale bar: 40 μm. In panel B, PANDAS serum incubation reduced phosphorylation levels of rpS6 in striatal CINs, relative to control serum incubation (unpaired t test,  $t=4.726$ ,  $df=20$ ,  $p=0.0001$ ); all values are normalized to slices incubated in parallel in saline with no serum. In panel C, serum incubation did not alter ChAT levels in the striatal slices. In panel D, the phosphorylation level of rpS6 correlated negatively with IgG binding to CINs in striatal slices (measured separately after incubation with the same sera; see Figure 1) ( $r^2=0.319$ ,  $p=0.006$ )—that is, higher IgG binding corresponds to a greater reduction in cell activity. In panel E, for each age- and gender-matched PANDAS-control pair, the PANDAS-control difference in IgG binding to striatal CINs correlated negatively with the difference in P-rpS6 after serum incubation ( $r^2=0.428$ ,  $p=0.029$ )—that is, greater differential IgG binding corresponds to greater comparative reduction in CIN P-rpS6. Panel F presents confocal images of co-staining of P-rpS6 (green) and

**FIGURE 4. Association of reduction in PANDAS IgG binding to cholinergic interneurons with decreases in CY-BOCS score after IVIG treatment<sup>a</sup>**



<sup>a</sup> CY-BOCS=Children's Yale-Brown Obsessive Compulsive Scale; IVIG=intravenous immunoglobulin. Sera were collected at baseline (pre-IVIG) and 6–12 weeks after IVIG treatment (post-IVIG) and tested for cholinergic interneuron (CIN) binding. Panel A presents representative images of co-staining of anti-human IgG (green) and anti-ChAT (choline acetyltransferase) (red) before and after IVIG treatment. "Merge" images combine both channels to illustrate overlap. Arrowheads indicate antibody binding to CINs. Scale bar: 40  $\mu$ m. In panel B, IVIG treatment resulted in decreased PANDAS IgG binding to CINs in the original five sera (paired t test,  $t=6.870$ ,  $df=4$ ,  $p=0.002$ ); this constitutes a technical replication of our previous analysis of the same samples, using a different assay (47). In panel C, the change in IgG binding to striatal CINs correlated with symptom improvement, although the difference did not reach statistical significance ( $r^2=0.753$ ,  $p=0.057$ ). In panel D, IVIG treatment similarly produced decreased PANDAS IgG binding to CINs in the second cohort ( $t=5.413$ ,  $df=5$ ,  $p=0.003$ ). In panel E, change in IgG binding to striatal CINs correlated significantly with symptom improvement in the second cohort ( $r^2=0.747$ ,  $p=0.026$ ). In panel F, the consistent effect of IVIG treatment across the two cohorts was particularly apparent in pooled data ( $t=8.191$ ,  $df=10$ ,  $p<0.0001$ ). In panel G, in pooled data, the correlation between change in serum IgG binding to CINs and improvement in symptoms was particularly robust ( $r^2=0.762$ ,  $p=0.0005$ ). Each data point represents the mean value obtained from four to six mice for one serum. For each group,  $N=5$  in panels B and C,  $N=6$  in panels D and E, and  $N=11$  in panels F and G. Dotted lines in correlation analyses indicate 95% confidence intervals. The first cohort was independently characterized in our previous pilot study (47).

\* $p<0.05$ . \*\* $p<0.01$ . \*\*\* $p<0.001$ .

consistent reduction in antibody binding to CINs (Figure 4B; see also Figure S19A in the online supplement). The pre- to posttreatment change in antibody binding to CINs correlated positively with symptom improvement (change in CY-BOCS score), although the difference did not reach statistical significance ( $p=0.057$ ) (Figure 4C). This constitutes a technical replication of our previous work on these sera using an in vivo antibody binding assay (47).

We repeated this analysis in the second cohort of six PANDAS patients and found a similar reduction in IgG binding to CINs after IVIG treatment (Figure 4D). The change in

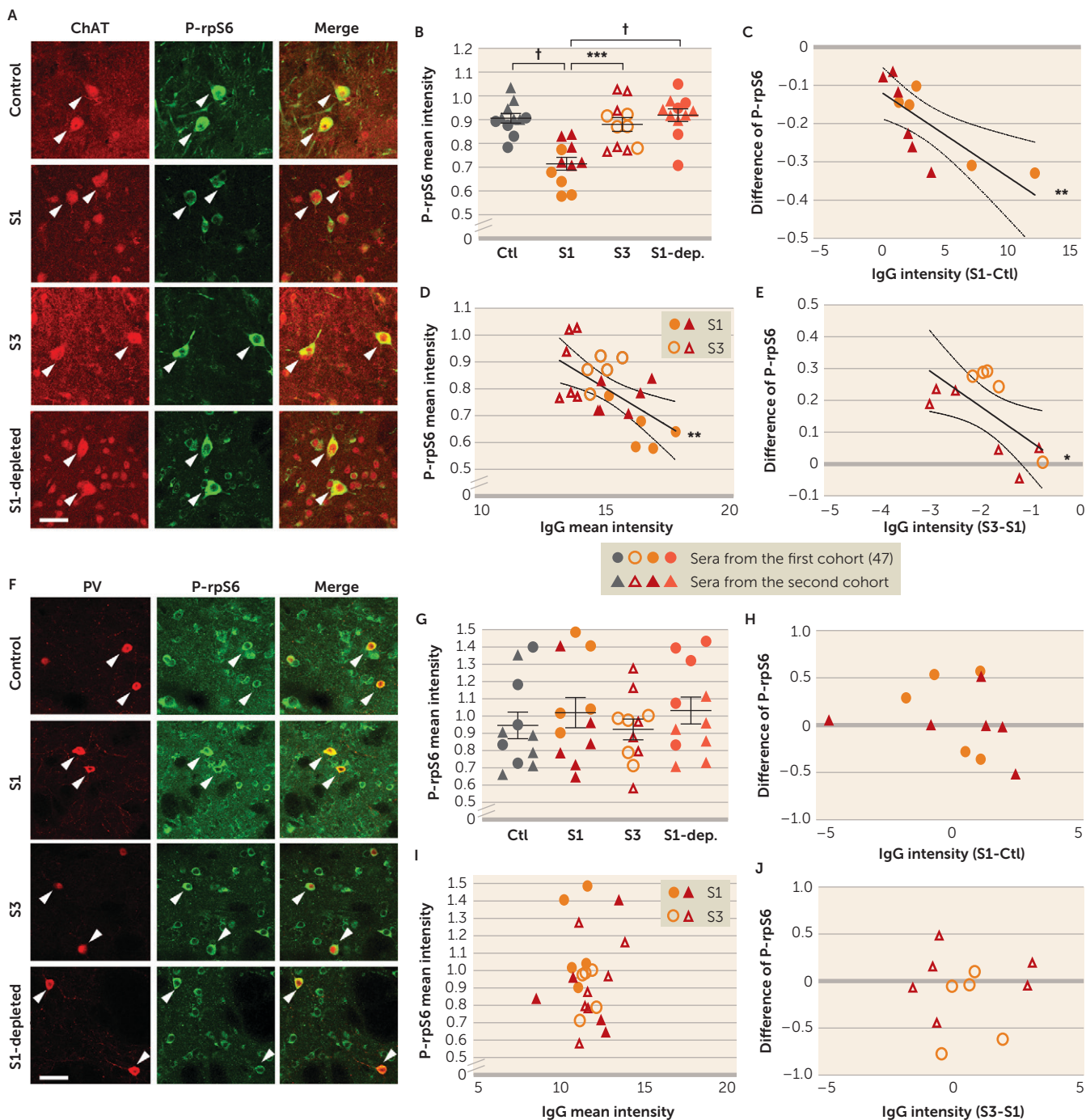
antibody binding to CINs correlated significantly with the change in CY-BOCS score in this second cohort (Figure 4E). In pooled data, IVIG significantly decreased IgG deposition onto CINs (Figure 4F). The decline in antibody binding correlated robustly with symptom improvement (Figure 4G).

To test the specificity of this change, we examined whether PANDAS IgG binding to other neurons would be altered after IVIG. There was no pre- to posttreatment change in IgG binding to striatal PV-positive neurons in the original cohort, the replication cohort, or the pooled data (see Figures S14B,D,F and S19B in the online supplement). There was no correlation

parvalbumin (PV) (red) in striatal slices after serum treatment. Arrowheads indicate P-rpS6/PV co-staining. Scale bar: 40  $\mu$ m. In panel G, PANDAS serum did not change P-rpS6 levels in striatal PV-interneurons (unpaired t test,  $t=0.393$ ,  $df=20$ ,  $p=0.7$ ). In panel H, serum incubation did not alter parvalbumin levels in the striatal slices. In panel I, there was no correlation between P-rpS6 levels and IgG binding to PV-interneurons in striatal slices. In panel J, for each age- and gender-matched PANDAS-control pair, the difference in IgG binding (PANDAS-control) to striatal PV-interneurons did not correlate with change in P-rpS6 after serum incubation.  $N=11$  for each group. The first cohort was independently characterized in our previous pilot study (47).

\* $p<0.05$ . \*\* $p<0.01$ . \*\*\* $p<0.001$ .

**FIGURE 5. Elimination, by IgG depletion and after IVIG treatment, of PANDAS serum’s ability to reduce spontaneous activity in striatal cholinergic interneurons in acute brain slices<sup>a</sup>**



<sup>a</sup> Acute mouse striatal slices were treated with sera collected at baseline (S1) and 6–12 weeks after intravenous immunoglobulin (IVIG) treatment (as in Figure 4; time point S3 in Figure S1 in the online supplement), with IgG-depleted S1 serum (S1-dep.) or with serum from matched control subjects (Ctl). Panel A presents confocal images of co-staining of anti-phospho-rpS6 (green) and anti-ChAT (choline acetyltransferase) (red). “Merge” images combine both channels to illustrate overlap. Arrowheads indicate P-rpS6/ChAT co-labeled cholinergic interneurons (CINs). Scale bar: 40  $\mu$ m. In panel B, pre-IVIG PANDAS serum (S1) reduced phosphorylation levels of rpS6 in striatal CINs compared with control, replicating Figure 3. This effect is lost in serum collected after IVIG treatment (S3) and by IgG depletion in S1 serum (S1-dep.) (one-way analysis of variance [ANOVA]:  $F=13.43$ ,  $df=3$ ,  $40$ ,  $p<0.0001$ ; pairwise comparisons by Tukey’s post hoc test: significance indicated by asterisks and dagger). In panel C, for each age- and gender-matched pre-IVIG PANDAS-control pair, the difference (S1–Ctl) in IgG binding to striatal CINs correlated negatively with change in P-rpS6 after serum incubation ( $r^2=0.564$ ,  $p=0.008$ ), consistent with the results in Figure 3E. In panel D, in pre-IVIG (S1) and post-IVIG (S3) PANDAS serum-treated slices, P-rpS6 levels correlated with IgG binding to CINs in striatal slices, measured previously (Figure 4F) ( $r^2=0.346$ ,  $p=0.004$ ). In panel E, for each pre-IVIG and post-IVIG PANDAS pair, the difference (S3–S1) in IgG binding to striatal CINs (Figure 4) correlated negatively with difference (S3–S1) in P-rpS6 after serum incubation ( $r^2=0.440$ ,  $p=0.026$ ). Panel F presents confocal images of co-staining of P-rpS6 (green) and PV (parvalbumin) (red) in striatal slices after serum treatment. Arrowheads indicate P-rpS6/PV co-staining. Scale bar: 40  $\mu$ m. In panel G, P-rpS6 levels in striatal PV-interneurons remained unchanged after serum

between pre- to posttreatment change in IgG binding and change in CY-BOCS score (see Figure S14C,E,G). Similarly, there was no alteration in IgG binding to cholinergic neurons in the medial septum after IVIG treatment (see Figures S14I,K,M and S19C) and no correlation between change in septal cholinergic neuron binding and change in CY-BOCS score (see Figure S14J,L,N).

### Prevention of the Effect of PANDAS Serum Pretreatment by IVIG Treatment and IgG Depletion on CIN Activity in Acute Striatal Slices

PANDAS serum-induced change in CIN activity (Figure 3) may be due to antibody binding to CINs (Figure 1) or to other factors in the serum. To investigate whether IgG binding is necessary for the change in activity, we repeated the treatment of acute brain slices with control and PANDAS sera (pre-IVIG, S1) with two additional experimental groups: matched post-IVIG PANDAS sera (post-IVIG, S3) and IgG-depleted pre-IVIG PANDAS sera (“S1-depleted”; see Figure S15 in the online supplement). PANDAS serum (S1) reduced P-rpS6 levels in striatal CINs relative to control serum (Figure 5A,B, replicating Figure 3B). The difference between PANDAS and control IgG binding to CINs (Figure 1) again correlated with the PANDAS-control difference in P-rpS6 after serum incubation (Figure 5C, replicating Figure 3E). In contrast, neither post-IVIG sera nor IgG-depleted baseline PANDAS serum reduced CIN P-rpS6 (Figure 5A,B). IgG binding of pre- and post-IVIG PANDAS sera (S1 and S3) to CINs correlated negatively with P-rpS6 levels after serum incubation (Figure 5D). The difference between IgG binding of baseline and post-IVIG treatment PANDAS serum correlated with the pre- to posttreatment difference in P-rpS6 levels after serum incubation (Figure 5E).

We also examined P-rpS6 levels in PV-expressing interneurons after serum treatment. Again, we found no difference between control and PANDAS groups (Figure 5F–H; compare with Figure 3G,J). Moreover, IVIG treatment and IgG depletion did not alter P-rpS6 levels in PV-interneurons (Figure 5F,G). No correlation was found between S1 and S3 sera IgG binding to PV-interneurons and P-rpS6 levels (Figure 5I) or between the difference in S1 and S3 IgG binding to PV-interneurons and the difference in P-rpS6 levels (Figure 5J). Serum treatment did not have any effect on ChAT or PV staining (data not shown).

## DISCUSSION

An autoimmune pathophysiology has been proposed for PANDAS but remains unproven (5–7). While a number of

possible pathogenic antibody targets have been described, none has been consistently replicated, and how the binding of antibodies to brain targets leads to symptoms remains unclear (8, 9, 15–18, 61–63). Our findings, here and in our previously published pilot study (47), reveal a hitherto unrecognized target for antibodies in these patients: the cholinergic interneurons (CINs) of the striatum. Our functional data (Figures 3 and 5) suggest that these antibodies can bind to CINs and reduce their activity, thereby disrupting the normal function of the corticostriatal circuitry.

Disruption of CINs has previously been implicated in Tourette’s syndrome, and in repetitive behavioral pathology more generally. Specifically, CINs are reduced in number in the striatum of adults with refractory Tourette’s syndrome (42, 43). Experimental depletion of these neurons in developmentally normal mice produces elevated grooming and repetitive behaviors, suggesting a causal relationship between this deficit and the development of relevant symptoms (45, 46). These previous, independent results make CIN dysregulation an inherently plausible locus of pathology in PANDAS.

The consistency and specificity of elevated antibody binding to CINs, but not other examined cells, is striking. We found elevated IgG binding to mouse striatal CINs in 27 children with PANDAS, across three independent cohorts of patients, compared with age- and gender-matched control subjects (Figure 1B). In conjunction with our previous results (47), the effect has now been seen using two different experimental approaches (in vivo and ex vivo antibody delivery), with both confocal and standard fluorescent imaging, with two different quantification strategies, in three different primary experimenters’ hands, with blinding to experimental condition. There is, with equal consistency, no elevated binding to two classes of GABAergic interneuron in the striatum (Figure 1D; see also Figure S6A in the online supplement) (47). Moreover, we confirmed these findings in human brains: 11 PANDAS sera showed elevated IgG binding to CINs in both caudate and putamen, compared with matched control subjects (Figure 2B,D), with no difference between groups in IgG binding to PV-interneurons (Figure 2F,H). It is of course possible that differential binding to other cell types would be seen in a more exhaustive examination of different cell types throughout the brain; this is an important direction for future research.

We found no altered binding to D1R- or D2R-expressing medium spiny neurons of the striatum (see Figure S6D,G in the online supplement). Binding by PANDAS antibodies to both D1R and D2R has been investigated previously, using in vitro binding to denatured protein (17, 18) or to heterologous cells overexpressing dopamine receptors (64). D2R is present on CINs and thus could explain elevated CIN binding.

---

incubation (one-way ANOVA,  $F=0.497$ ,  $df=3, 40$ ,  $p>0.7$ ). In panel H, for each age- and gender-matched pre-IVIG PANDAS-control pair, the difference in IgG binding (S1–Ctl) to striatal PV-interneurons did not correlate with change in P-rpS6 after serum incubation ( $r^2=0.061$ ,  $p>0.4$ ), consistent with the results in Figure 3J. In panel I, in pre-IVIG (S1) and post-IVIG (S3) PANDAS serum-treated slices, P-rpS6 levels correlated with IgG binding to PV-interneurons in striatal slices ( $r^2=0.009$ ,  $p>0.6$ ). In panel J, for each pre-IVIG and post-IVIG PANDAS pair, the difference (S3–S1) in IgG binding to striatal PV-interneurons did not correlate with change in P-rpS6 after serum incubation ( $r^2=0.001$ ,  $p>0.9$ ).  $N=11$  for each group. The first cohort was independently characterized in our previous pilot study (47).

\* $p<0.05$ . \*\* $p<0.01$ . \*\*\* $p<0.001$ . † $p<0.0001$ .

The lack of any change in binding to D2R-expressing medium spiny neurons, however, argues against this possibility. We also see no elevated binding to cholinergic cells in the medial septum (Figure 1E), indicating that the abnormality does not generalize to cholinergic cells throughout the nervous system, or even the forebrain.

The specific molecular targets on striatal CINs that explain elevated binding by PANDAS IgG remain unclear. There may be a single molecular target on these cells that has eluded identification in previous studies, perhaps because it is present at low concentration in total striatal lysate (as CINs represent a small minority of the cells in the striatum). However, our experimental approach does not require that a single molecular target explain the observed binding in all patients; it is possible that there are multiple targets that can lead to similar binding patterns and similar pathophysiological effects in different patients. Such heterogeneity could further explain the lack of replication that has characterized efforts to identify specific antibodies on the basis of binding to specific molecules, rather than to cell types. We note that in these experiments (though not in our previous work [47]) tissue was permeabilized before application of serum, and thus both cell surface and intracellular antigens are accessible; surface antigens may be more relevant pathophysiological targets *in vivo*. Identification of the molecular targets of antibody binding in individual sera is an important future direction for this work.

In the third cohort of PANDAS patients, who were not selected for IVIG response (and some of whom were not treated with IVIG at all), we found a similar but statistically weaker increase in IgG binding to CINs. The somewhat attenuated effect in this third cohort suggests that it may be more heterogeneous, containing some subjects with IgG-mediated pathology similar to that present in the first cohorts but others with a different pathophysiology. Identification of the clinical correlates of elevated IgG binding to CINs, both in patients with PANDAS and in related diagnostic groups, is an important direction for future work.

Our results also show, for the first time, that PANDAS antibodies can affect CIN activity, providing critical support for the proposed pathophysiological mechanism. Specifically, we treated mouse striatal slices with PANDAS and control serum *ex vivo*, and we measured activity-dependent phosphorylation of ribosomal protein S6 (P-rpS6), a validated marker of neuronal activity in both CINs (57) and PV-expressing interneurons (58, 59). We found reduced P-rpS6 after treatment with 11 PANDAS sera, but not with matched control sera (Figure 3B). This effect is lost when IgG is depleted from PANDAS serum (Figure 5B), indicating that IgG binding is necessary for CIN inhibition. Importantly, there is no similar effect on PV-expressing interneurons (Figure 3G–J), further emphasizing the specificity of the effects on CINs seen throughout our study. Of course, we cannot exclude the possibility that antibodies in PANDAS sera can have other effects on PV-expressing interneurons not captured by this assay, or on other cells elsewhere in the brain.

Antibody-modulating therapies such as IVIG and plasmapheresis have shown promise in the treatment of PANDAS in some studies, though not in all (19–22). Our first two patient cohorts were drawn from a recent controlled study of IVIG treatment (21) (see Figure S1 in the online supplement). This allowed testing of serum collected before and after treatment (47). We found that IgG binding to CINs was reduced after IVIG treatment, and that this change correlated robustly with symptom improvement (Figure 4). Similarly, post-IVIG serum did not reduce CIN activity (Figure 5B); the change in antibody binding correlated with the change in ability to reduce CIN activity. Critically, there was no change in binding to PV-expressing interneurons in the striatum or in cholinergic cells of the medial septum after IVIG treatment (see Figure S14 in the online supplement).

As an additional measure of neuronal activity, we examined CIN response to bath neurotransmitter treatment *ex vivo* after incubation with PANDAS or control serum. PANDAS serum significantly attenuated AMPA-induced spike frequency (see Figure S12A,B in the online supplement). This may explain reduced P-rpS6 after PANDAS treatment (Figures 3 and 5), to the extent that glutamate tone contributes to basal CIN firing in our *ex vivo* preparation. PANDAS serum also modulated cellular responses to both dopamine and 5-HT. We were only able to perform these electrophysiological experiments with a single serum pair, because of limited supplies of clinical serum and the relatively large amounts needed for these studies. Nevertheless, in conjunction with the P-rpS6 staining data across 11 PANDAS samples and matched control subjects (Figure 3), these data indicate that PANDAS serum can reduce activity of CINs.

The downstream consequences of PANDAS IgG binding to CINs *in vivo* remain to be elucidated. We hypothesize that pathogenic PANDAS antibodies reduce CIN activity *in vivo*, as we have shown *ex vivo* (Figures 3 and 5; see also Figures S12 and S13 in the online supplement). This may functionally parallel the effect of reduced CIN number in adults with severe Tourette's syndrome (42, 43) and of experimental CIN disruption producing repetitive behavioral pathology in mice (45). CINs have been shown to differentially regulate D1R-expressing medium spiny neurons of the striatonigral (direct) pathway and D2R-expressing medium spiny neurons of the striatopallidal (indirect) pathway (65, 66) via muscarinic acetylcholine receptors (54, 67). The CINs interact with other neurotransmitter systems; they co-release glutamate (68) and drive dopamine and GABA release from dopamine terminals (69–71). CINs can also indirectly inhibit medium spiny neurons via their up-regulation of GABAergic interneuron activity (72–75). Thus, inhibition of CINs may lead to dysregulated striatal output through several mechanisms.

Dysfunction of basal ganglia occurs commonly in other autoimmune encephalitides. Functional brain imaging studies show basal ganglia hypermetabolism in patients with autoimmune encephalitis (76, 77). In anti-*N*-methyl-D-aspartate (NMDA) receptor encephalitis, loss of cortico-striatal inhibition

due to antibody-mediated inhibition of GABAergic interneurons has been postulated (78–80). In another rare autoimmune disorder, stiff-person syndrome, anti-GAD65 (81), and anti-amphiphysin (82) autoantibodies disrupt GABAergic inhibitory synaptic activity, which may underlie the pathophysiology of this disorder. Our findings suggest that a similar mechanism may be at play in PANDAS, with antibody binding to interneurons leading to an imbalance between excitatory and inhibitory synaptic transmission in the basal ganglia and thus to clinical symptoms. Importantly, we have not shown antibody binding to CINs to be specific to PANDAS; indeed, since PANDAS is a clinical entity and its diagnosis is not based on a clearly defined underlying pathophysiology, we think it unlikely that elevated CIN binding will correspond precisely with clinical diagnosis. This binding pattern may not be seen in all patients with a PANDAS diagnosis (as suggested by the overlap of PANDAS and control values in Figure 1), and a similar pathophysiology may contribute to other neuroinflammatory conditions. Systematic examination of interneuron binding across psychiatric and neurological diagnoses is an important future direction; such an examination will be facilitated by the identification of the associated molecular targets.

In this study, we tested PANDAS IgG binding to fixed mouse striatal slices and to human brain tissue, *ex vivo*. This differs from the *in vivo* infusion used in our pilot work (47). These two strategies ask subtly different questions. *In vivo* antibody infusion demonstrates that antibodies in PANDAS sera can bind to CINs in intact brain, under physiological conditions, over days. The *ex vivo* approach used here is less chronic, examining binding after an overnight incubation (Figures 1, 2, and 4) and functional effects after only 1 hour (Figures 3 and 5; see also Figures S12 and S13 in the online supplement). It allows better control of IgG concentration, which may vary between animals *in vivo*. It is less laborious, which allows for analysis of larger numbers of samples and the inclusion of additional controls. Importantly, the *ex vivo* approach permits, for the first time, examination of the functional effects of PANDAS serum on CIN activity (Figures 3 and 5; see also Figures S12 and S13).

We also used an automated method to quantify IgG binding to CINs and other neuronal types (see Figure S2 in the online supplement), which contrasts with the blinded manual counting used in our pilot work (47). This allowed us to count an order of magnitude more cells than previously. On the other hand, the effect size of the elevated binding of IgG to CINs in our pilot work ( $d=8.1$ ) was much higher than that we observed here ( $d=1.8$  in the first cohort and somewhat less in the others). The use of standard fluorescent imaging rather than confocal imaging, which allows us to count more cells at lower magnification, leads to higher background, which doubtless contributes to this smaller (though still large) effect size. Lower background in the *in vivo* work may also derive from the more chronic serum administration and the 5-day clearance period after antibody infusion (47), which may produce a better signal-to-noise ratio. Additionally, in our

previous work, we categorized individual cells as either positive or negative for IgG, which is an inherently nonlinear approach and may amplify between-group effects. The finding of qualitatively identical results using these two experimental approaches, despite these differences, increases confidence in the finding.

There are, of course, several limitations to this study. The sera are as clinically homogeneous as we could achieve, especially in the first two patient cohorts, with rigorous PANDAS diagnosis and a narrow age range. These design choices were made to maximize our ability to find a pathophysiological signal in a small, homogeneous sample, which can subsequently be investigated in more heterogeneous populations. This approach has been fruitful in investigations of other autoimmune neural pathologies (83). We examined binding to both mouse and human striatal tissue, but in both cases this tissue was from adults; it is possible that more or different binding would be seen on pediatric tissue. We focused on a specific brain region (the striatum) and on specific cell types, based on *a priori* considerations; it is possible that a more comprehensive survey would additionally reveal elevated binding by PANDAS IgG to other cells in other brain regions. And we focused on the ability of IgG to bind to interneurons but have not addressed the question of how these antibodies could access the brain in patients; this is an important, though distinct, topic for future research.

While the finding of elevated IgG binding to CINs documented here represents an exciting new insight into possible pathophysiological mechanisms in PANDAS, it would be premature to consider this a clinical assay. Overlap between PANDAS and control groups is substantial (Figure 1B), and the specificity and prognostic utility of elevated CIN binding remain to be established. Development of a diagnostic assay based on these results may require the identification of the molecular target(s) of antibody binding to CINs. This is an important future direction. Ultimately, the identification and replication of specific binding targets, and clarification of their relationship to particular patterns of symptoms or of treatment response, may help clarify the diagnostic landscape in PANDAS and PANS, in addition to providing clinically useful laboratory tests.

In conclusion, we found that PANDAS antibodies showed elevated binding to striatal CINs but not several other neuronal types (47), declined in parallel with symptom improvement after IVIG treatment, and reduced the activity of CINs—and perhaps altered their response to several neurotransmitters—*ex vivo*. This supports a novel hypothesis for the pathophysiology of PANDAS, which in turn suggests important directions for future research. Identifying cellular targets of pathogenic antibodies in PANDAS holds promise for validation of the diagnosis and for the identification of molecular targets for future treatment development.

#### AUTHOR AND ARTICLE INFORMATION

Department of Psychiatry (Xu, Liu, Fahey, Frick, Duman, Williams, Pittenger), Child Study Center (Leckman, Vaccarino, Pittenger), Department of Pediatrics (Leckman), and Department of Neuroscience (Vaccarino),

Yale University School of Medicine, New Haven, Conn.; Hunter James Kelly Research Institute, University at Buffalo, State University of New York, Buffalo (Frick); Department of Psychiatry, Massachusetts General Hospital and Harvard Medical School (Williams), Boston; Pediatrics and Developmental Neuroscience Branch, NIMH, Bethesda, Md. (Swedo); PANDAS Physicians Network (Swedo); and Interdepartmental Neuroscience Program, Yale University, New Haven, Conn. (Pittenger).

Send correspondence to Dr. Pittenger (christopher.pittenger@yale.edu) and Dr. Xu (jian.xu@yale.edu).

Dr. Duman died on February 21, 2020.

Supported by NIH grants R01NS101104 and R21MH109700 and NIH contract HHSN271201800709P (Dr. Pittenger), by the NIMH Intramural Research Program (Dr. Swedo), and by the Avielle Foundation (Ms. Fahey). Support was also received from the State of Connecticut through its support of the Ribicoff Research Facilities at the Connecticut Mental Health Center.

The authors thank Jessica Lenington for assistance with human tissue processing, Margaret Pekar and Betsy D'Amico for assistance with serum handling and organization, Betsy D'Amico for mouse genotyping and management, and other laboratory members for helpful discussions and critical reading of the manuscript.

Dr. Duman served as a consultant for Johnson & Johnson, Naurex, and Taisho and received grant support from Allergan, Eli Lilly, Johnson & Johnson, Lundbeck, Naurex, Navitor, and Taisho. Dr. Pittenger has served as a consultant for Biohaven Pharmaceuticals, Brainsway Therapeutics, and Teva Pharmaceuticals, and he has performed research under contract with Biohaven and with Blackthorn Therapeutics. The other authors report no financial relationships with commercial interests.

Received July 6, 2019; revisions received January 30 and March 12, 2020; accepted March 23, 2020; published online June 16, 2020.

## REFERENCES

- Weissman MM, Bland RC, Canino GJ, et al: The cross national epidemiology of obsessive compulsive disorder. *J Clin Psychiatry* 1994; 55(suppl):5-10
- Ruscio AM, Stein DJ, Chiu WT, et al: The epidemiology of obsessive-compulsive disorder in the National Comorbidity Survey Replication. *Mol Psychiatry* 2010; 15:53-63
- Swedo SE, Leckman JF, Rose NR: From research subgroup to clinical syndrome: modifying the PANDAS criteria to describe PANS (pediatric acute-onset neuropsychiatric syndrome). *Pediatr Ther* 2012; 2:113.
- Singer HS, Gilbert DL, Wolf DS, et al: Moving from PANDAS to CANS. *J Pediatr* 2012; 160:725-731
- Swedo SE, Leonard HL, Garvey M, et al: Pediatric autoimmune neuropsychiatric disorders associated with streptococcal infections: clinical description of the first 50 cases. *Am J Psychiatry* 1998; 155:264-271
- Murphy TK, Patel PD, McGuire JF, et al: Characterization of the pediatric acute-onset neuropsychiatric syndrome phenotype. *J Child Adolesc Psychopharmacol* 2015; 25:14-25
- Chang K, Frankovich J, Cooperstock M, et al: Clinical evaluation of youth with pediatric acute-onset neuropsychiatric syndrome (PANS): recommendations from the 2013 PANS Consensus Conference. *J Child Adolesc Psychopharmacol* 2015; 25:3-13
- Kirvan CA, Swedo SE, Heuser JS, et al: Mimicry and autoantibody-mediated neuronal cell signaling in Sydenham chorea. *Nat Med* 2003; 9:914-920
- Kirvan CA, Swedo SE, Kurahara D, et al: Streptococcal mimicry and antibody-mediated cell signaling in the pathogenesis of Sydenham's chorea. *Autoimmunity* 2006; 39:21-29
- Swedo SE: Sydenham's chorea: a model for childhood autoimmune neuropsychiatric disorders. *JAMA* 1994; 272:1788-1791
- Swedo SE, Rapoport JL, Cheslow DL, et al: High prevalence of obsessive-compulsive symptoms in patients with Sydenham's chorea. *Am J Psychiatry* 1989; 146:246-249
- Asbahr FR, Garvey MA, Snider LA, et al: Obsessive-compulsive symptoms among patients with Sydenham chorea. *Biol Psychiatry* 2005; 57:1073-1076
- Witebsky E, Rose NR, Terplan K, et al: Chronic thyroiditis and autoimmunization. *J Am Med Assoc* 1957; 164:1439-1447
- Rose NR, Bona C: Defining criteria for autoimmune diseases (Witebsky's postulates revisited). *Immunol Today* 1993; 14:426-430
- Kirvan CA, Swedo SE, Snider LA, et al: Antibody-mediated neuronal cell signaling in behavior and movement disorders. *J Neuroimmunol* 2006; 179:173-179
- Kirvan CA, Cox CJ, Swedo SE, et al: Tubulin is a neuronal target of autoantibodies in Sydenham's chorea. *J Immunol* 2007; 178:7412-7421
- Ben-Pazi H, Stoner JA, Cunningham MW: Dopamine receptor autoantibodies correlate with symptoms in Sydenham's chorea. *PLoS One* 2013; 8:e73516
- Cox CJ, Sharma M, Leckman JF, et al: Brain human monoclonal autoantibody from Sydenham chorea targets dopaminergic neurons in transgenic mice and signals dopamine D2 receptor: implications in human disease. *J Immunol* 2013; 191:5524-5541
- Perlmutter SJ, Leitman SF, Garvey MA, et al: Therapeutic plasma exchange and intravenous immunoglobulin for obsessive-compulsive disorder and tic disorders in childhood. *Lancet* 1999; 354:1153-1158
- Garvey MA, Snider LA, Leitman SF, et al: Treatment of Sydenham's chorea with intravenous immunoglobulin, plasma exchange, or prednisone. *J Child Neurol* 2005; 20:424-429
- Williams KA, Swedo SE, Farmer CA, et al: Randomized, controlled trial of intravenous immunoglobulin for pediatric autoimmune neuropsychiatric disorders associated with streptococcal infections. *J Am Acad Child Adolesc Psychiatry* 2016; 55:860-867.e2
- Sigra S, Hesselmark E, Bejerot S: Treatment of PANDAS and PANS: a systematic review. *Neurosci Biobehav Rev* 2018; 86:51-65
- Snider LA, Lougee L, Slattery M, et al: Antibiotic prophylaxis with azithromycin or penicillin for childhood-onset neuropsychiatric disorders. *Biol Psychiatry* 2005; 57:788-792
- Garvey MA, Perlmutter SJ, Allen AJ, et al: A pilot study of penicillin prophylaxis for neuropsychiatric exacerbations triggered by streptococcal infections. *Biol Psychiatry* 1999; 45:1564-1571
- Kurlan R, Kaplan EL: The pediatric autoimmune neuropsychiatric disorders associated with streptococcal infection (PANDAS) etiology for tics and obsessive-compulsive symptoms: hypothesis or entity? Practical considerations for the clinician. *Pediatrics* 2004; 113:883-886
- Yaddanapudi K, Hornig M, Serge R, et al: Passive transfer of streptococcus-induced antibodies reproduces behavioral disturbances in a mouse model of pediatric autoimmune neuropsychiatric disorders associated with streptococcal infection. *Mol Psychiatry* 2010; 15:712-726
- Lotan D, Benhar I, Alvarez K, et al: Behavioral and neural effects of intra-striatal infusion of anti-streptococcal antibodies in rats. *Brain Behav Immun* 2014; 38:249-262
- Pauls DL, Abramovitch A, Rauch SL, et al: Obsessive-compulsive disorder: an integrative genetic and neurobiological perspective. *Nat Rev Neurosci* 2014; 15:410-424
- Fernandez TV, Leckman JF, Pittenger C: Genetic susceptibility in obsessive-compulsive disorder. *Handb Clin Neurol* 2018; 148:767-781
- Menzies L, Chamberlain SR, Laird AR, et al: Integrating evidence from neuroimaging and neuropsychological studies of obsessive-compulsive disorder: the orbitofronto-striatal model revisited. *Neurosci Biobehav Rev* 2008; 32:525-549
- Bostan AC, Strick PL: The basal ganglia and the cerebellum: nodes in an integrated network. *Nat Rev Neurosci* 2018; 19:338-350
- Harrison BJ, Soriano-Mas C, Pujol J, et al: Altered corticostriatal functional connectivity in obsessive-compulsive disorder. *Arch Gen Psychiatry* 2009; 66:1189-1200
- Radua J, Mataix-Cols D: Voxel-wise meta-analysis of grey matter changes in obsessive-compulsive disorder. *Br J Psychiatry* 2009; 195:393-402

34. Pittenger C, Bloch MH, Williams K: Glutamate abnormalities in obsessive compulsive disorder: neurobiology, pathophysiology, and treatment. *Pharmacol Ther* 2011; 132:314–332
35. Anticevic A, Hu S, Zhang S, et al: Global resting-state functional magnetic resonance imaging analysis identifies frontal cortex, striatal, and cerebellar dysconnectivity in obsessive-compulsive disorder. *Biol Psychiatry* 2014; 75:595–605
36. Gerfen CR, Bolam JP: The neuroanatomical organization of the basal ganglia, in *Handbook of Behavioral Neuroscience*, vol 20. London, Elsevier, 2010, pp 3–28
37. Kreitzer AC: Physiology and pharmacology of striatal neurons. *Annu Rev Neurosci* 2009; 32:127–147
38. Tepper JM, Bolam JP: Functional diversity and specificity of neostriatal interneurons. *Curr Opin Neurobiol* 2004; 14:685–692
39. Apicella P: Leading tonically active neurons of the striatum from reward detection to context recognition. *Trends Neurosci* 2007; 30: 299–306
40. Burguière E, Monteiro P, Mallet L, et al: Striatal circuits, habits, and implications for obsessive-compulsive disorder. *Curr Opin Neurobiol* 2015; 30:59–65
41. Rapanelli M, Frick LR, Pittenger C: The role of interneurons in autism and Tourette syndrome. *Trends Neurosci* 2017; 40: 397–407
42. Kataoka Y, Kalanithi PS, Grantz H, et al: Decreased number of parvalbumin and cholinergic interneurons in the striatum of individuals with Tourette syndrome. *J Comp Neurol* 2010; 518: 277–291
43. Lenington JB, Coppola G, Kataoka-Sasaki Y, et al: Transcriptome analysis of the human striatum in Tourette syndrome. *Biol Psychiatry* 2016; 79:372–382
44. Kalanithi PS, Zheng W, Kataoka Y, et al: Altered parvalbumin-positive neuron distribution in basal ganglia of individuals with Tourette syndrome. *Proc Natl Acad Sci USA* 2005; 102:13307–13312
45. Xu M, Kobets A, Du JC, et al: Targeted ablation of cholinergic interneurons in the dorsolateral striatum produces behavioral manifestations of Tourette syndrome. *Proc Natl Acad Sci USA* 2015; 112: 893–898
46. Rapanelli M, Frick LR, Xu M, et al: Targeted interneuron depletion in the dorsal striatum produces autism-like behavioral abnormalities in male but not female mice. *Biol Psychiatry* 2017; 82: 194–203
47. Frick LR, Rapanelli M, Jindachomthong K, et al: Differential binding of antibodies in PANDAS patients to cholinergic interneurons in the striatum. *Brain Behav Immun* 2018; 69:304–311
48. Scahill L, Riddle MA, McSwiggin-Hardin M, et al: Children's Yale-Brown Obsessive Compulsive Scale: reliability and validity. *J Am Acad Child Adolesc Psychiatry* 1997; 36:844–852
49. Bateup HS, Svenningsson P, Kuroiwa M, et al: Cell type-specific regulation of DARPP-32 phosphorylation by psychostimulant and antipsychotic drugs. *Nat Neurosci* 2008; 11:932–939
50. Rapanelli M, Frick L, Jindachomthong K, et al: Striatal signaling regulated by the H3R histamine receptor in a mouse model of tic pathophysiology. *Neuroscience* 2018; 392:172–179
51. Ting JT, Daigle TL, Chen Q, et al: Acute brain slice methods for adult and aging animals: application of targeted patch clamp analysis and optogenetics. *Methods Mol Biol* 2014; 1183:221–242
52. Liu RJ, Aghajanian GK: Stress blunts serotonin- and hypocretin-evoked EPSCs in prefrontal cortex: role of corticosterone-mediated apical dendritic atrophy. *Proc Natl Acad Sci USA* 2008; 105:359–364
53. Rapanelli M, Frick LR, Horn KD, et al: The histamine H3 receptor differentially modulates mitogen-activated protein kinase (MAPK) and Akt signaling in striatonigral and striatopallidal neurons. *J Biol Chem* 2016; 291:21042–21052
54. Lim SA, Kang UJ, McGehee DS: Striatal cholinergic interneuron regulation and circuit effects. *Front Synaptic Neurosci* 2014; 6:22
55. Gonzales KK, Smith Y: Cholinergic interneurons in the dorsal and ventral striatum: anatomical and functional considerations in normal and diseased conditions. *Ann N Y Acad Sci* 2015; 1349:1–45
56. Martos YV, Braz BY, Beccaria JP, et al: Compulsive social behavior emerges after selective ablation of striatal cholinergic interneurons. *J Neurosci* 2017; 37:2849–2858
57. Bertran-Gonzalez J, Chieng BC, Laurent V, et al: Striatal cholinergic interneurons display activity-related phosphorylation of ribosomal protein S6. *PLoS One* 2012; 7:e53195
58. Knight ZA, Tan K, Birsoy K, et al: Molecular profiling of activated neurons by phosphorylated ribosome capture. *Cell* 2012; 151: 1126–1137
59. Pirbhoy PS, Farris S, Steward O: Synaptic activation of ribosomal protein S6 phosphorylation occurs locally in activated dendritic domains. *Learn Mem* 2016; 23:255–269
60. Kovacevic M, Grant P, Swedo SE: Use of intravenous immunoglobulin in the treatment of twelve youths with pediatric autoimmune neuropsychiatric disorders associated with streptococcal infections. *J Child Adolesc Psychopharmacol* 2015; 25:65–69
61. Singer HS, Hong JJ, Yoon DY, et al: Serum autoantibodies do not differentiate PANDAS and Tourette syndrome from controls. *Neurology* 2005; 65:1701–1707
62. Morris CM, Pardo-Villamizar C, Gause CD, et al: Serum autoantibodies measured by immunofluorescence confirm a failure to differentiate PANDAS and Tourette syndrome from controls. *J Neurol Sci* 2009; 276:45–48
63. Brilot F, Merheb V, Ding A, et al: Antibody binding to neuronal surface in Sydenham chorea, but not in PANDAS or Tourette syndrome. *Neurology* 2011; 76:1508–1513
64. Dale RC, Merheb V, Pillai S, et al: Antibodies to surface dopamine-2 receptor in autoimmune movement and psychiatric disorders. *Brain* 2012; 135:3453–3468
65. Nelson AB, Kreitzer AC: Reassessing models of basal ganglia function and dysfunction. *Annu Rev Neurosci* 2014; 37:117–135
66. Lanciego JL, Luquin N, Obeso JA: Functional neuroanatomy of the basal ganglia. *Cold Spring Harb Perspect Med* 2012; 2:a009621
67. Ding JB, Guzman JN, Peterson JD, et al: Thalamic gating of corticostriatal signaling by cholinergic interneurons. *Neuron* 2010; 67: 294–307
68. Higley MJ, Gittis AH, Oldenburg IA, et al: Cholinergic interneurons mediate fast VGLUT3-dependent glutamatergic transmission in the striatum. *PLoS One* 2011; 6:e19155
69. Nelson AB, Hammack N, Yang CF, et al: Striatal cholinergic interneurons drive GABA release from dopamine terminals. *Neuron* 2014; 82:63–70
70. Zhou FM, Liang Y, Dani JA: Endogenous nicotinic cholinergic activity regulates dopamine release in the striatum. *Nat Neurosci* 2001; 4:1224–1229
71. Threlfell S, Lalic T, Platt NJ, et al: Striatal dopamine release is triggered by synchronized activity in cholinergic interneurons. *Neuron* 2012; 75:58–64
72. Koós T, Tepper JM: Dual cholinergic control of fast-spiking interneurons in the neostriatum. *J Neurosci* 2002; 22:529–535
73. English DF, Ibanez-Sandoval O, Stark E, et al: GABAergic circuits mediate the reinforcement-related signals of striatal cholinergic interneurons. *Nat Neurosci* 2011; 15:123–130
74. Faust TW, Assous M, Tepper JM, et al: Neostriatal GABAergic interneurons mediate cholinergic inhibition of spiny projection neurons. *J Neurosci* 2016; 36:9505–9511
75. Faust TW, Assous M, Shah F, et al: Novel fast adapting interneurons mediate cholinergic-induced fast GABA<sub>A</sub> inhibitory postsynaptic currents in striatal spiny neurons. *Eur J Neurosci* 2015; 42: 1764–1774
76. Maeder-Ingvar M, Prior JO, Irani SR, et al: FDG-PET hyperactivity in basal ganglia correlating with clinical course in anti-NDMA-R antibodies encephalitis. *J Neurol Neurosurg Psychiatry* 2011; 82: 235–236

77. Turpin S, Martineau P, Levasseur MA, et al: 18F-Fluorodeoxyglucose positron emission tomography with computed tomography (FDG PET/CT) findings in children with encephalitis and comparison to conventional imaging. *Eur J Nucl Med Mol Imaging* 2019; 46:1309–1324
78. Kleinig TJ, Thompson PD, Matar W, et al: The distinctive movement disorder of ovarian teratoma-associated encephalitis. *Mov Disord* 2008; 23:1256–1261
79. Dalmau J, Gleichman AJ, Hughes EG, et al: Anti-NMDA-receptor encephalitis: case series and analysis of the effects of antibodies. *Lancet Neurol* 2008; 7:1091–1098
80. Mohammad SS, Fung VS, Grattan-Smith P, et al: Movement disorders in children with anti-NMDAR encephalitis and other autoimmune encephalopathies. *Mov Disord* 2014; 29:1539–1542
81. Blum P, Jankovic J: Stiff-person syndrome: an autoimmune disease. *Mov Disord* 1991; 6:12–20
82. Geis C, Weishaupt A, Hallermann S, et al: Stiff person syndrome-associated autoantibodies to amphiphysin mediate reduced GABAergic inhibition. *Brain* 2010; 133:3166–3180
83. Fujihara K: Neuromyelitis optica spectrum disorders: still evolving and broadening. *Curr Opin Neurol* 2019; 32:385–394